Geomechanics and Engineering, *Vol. 41, No. 1 (2025) 151-163*
https://doi.org/10.12989/gae.2025.41.1.151

Subsidence characterization of karst sinkholes using satellite remote sensing: A Missouri case study

Arip Syaripudin Nur[1a], Yong Je Kim*[1], Boo Hyun Nam[2b], Kyungwon Park[2c] and Jinwoo An[3d]

[1]*Department of Civil and Environmental Engineering, Lamar University, Beaumont, TX 77710, USA*
[2]*Department of Civil Engineering, Kyung Hee University, Yongin-si, Gyenggi-do 17104,Republic of Korea*
[3]*Department of Civil Engineering, The University of Texas Rio Grande Valley, Edinburg, TX 78541, USA*

(*Received December 7, 2024, Revised February 27, 2025, Accepted March 5, 2025*)

Abstract. Greene County in Missouri has experienced a significant increase in sinkhole occurrences over recent decades due to its karst geology. This study focuses on investigating ground subsidence related to karst sinkholes using satellite-based remote sensing techniques and aims to develop a sinkhole susceptibility map utilizing Geographic Information System (GIS) methodologies. Interferometric Synthetic Aperture Radar (InSAR) data from Sentinel-1 satellites, covering the period from 2018 to 2020, were employed to detect and analyze ground deformation patterns. The InSAR analysis revealed an annual subsidence rate of up to 30 mm along the satellite's line-of-sight, indicating active ground movements in the region. To predict areas susceptible to future sinkhole development, a sinkhole inventory dataset was compiled from the Missouri Department of Natural Resources (MoDNR), and an Artificial Neural Network (ANN) machine learning model was applied. Topographic conditioning factors were derived from high-resolution Light Detection and Ranging (LiDAR) data to enhance the predictive modeling. The results demonstrated a strong correlation between areas of significant deformation detected by InSAR and regions identified as highly susceptible to sinkholes in the susceptibility map. Furthermore, newly identified sinkholes coincided with zones of high subsidence, validating the predictive capacity of the ANN model. This study underscores the effectiveness of integrating satellite remote sensing with machine learning techniques to detect subtle ground deformation and to map zones at risk of future sinkhole formation. The proposed approach offers valuable insights for sustainable urban development, land-use planning, and hazard mitigation strategies in karst regions like Greene County.

Keywords: GIS; InSAR remote sensing; karst subsidence; machine learning; sinkhole susceptibility

1. Introduction

Sinkholes are depressions or holes in the ground caused by the collapse of surface layers, representing significant geological hazards in many regions globally (Nam and Shamet 2020). These features commonly form in areas underlain by soluble rocks such as limestone, dolomite, or gypsum. In these karst landscapes, water percolates through the soil and dissolves the underlying bedrock, gradually creating underground voids and cavities (Shamet *et al.* 2021). When the overlying ground material can no longer support itself due to the enlargement of these voids, it collapses, resulting in a sinkhole at the surface (Intrieri *et al.* 2015).

Missouri lies within the Springfield Plateau, part of the Ozark Physiographic Region in the United States. This region is characterized by the presence of Mississippian-age carbonate rocks, particularly the Burlington-Keokuk

Limestone, which is highly soluble and susceptible to karstification (Barner and Gouzie 2024). The extensive dissolution of this limestone has led to the development of over 14,000 documented sinkholes in the area. Additionally, features such as losing streams, springs, and caves further emphasize the region's geological susceptibility to karst processes (Kim *et al*. 2022).

Rapid urbanization in Greene County has heightened the risks associated with sinkhole formation. Limited availability of prime development areas has forced construction into regions inherently prone to sinkhole development, increasing the potential for structural damage to infrastructure, flooding, and contamination of groundwater resources (Talib *et al*. 2022). Development in proximity to sinkholes has exacerbated these problems, leading to increased pollution entering the shallow aquifer systems and causing significant economic and social impacts (Prete 2010). Sinkhole-related damages in the United States are estimated to exceed $304 million annually (Weary 2015), highlighting the critical need for effective sinkhole investigation and risk assessment strategies to ensure sustainable urban development.

Detecting sinkhole deformation prior to catastrophic collapse poses significant challenges, as early signs of subsidence are often subtle or imperceptible on the ground surface. Traditional geophysical methods such as ground-penetrating radar (GPR), electrical resistivity tomography (ERT), and shallow seismic surveys have been employed to

*Corresponding author, Assistant Professor
E-mail: ykim3@lamar.edu
[a]Ph.D. Student
[b]Professor
[c]Ph.D. Student
[d]Assistant Professor

ISSN: 2005-307X (Print), 2092-6219 (Online)

monitor sinkhole activity (Abdelmawla *et al*. 2023, Min and Yoon 2024, Song *et al.* 2023, Theron and Engelbrecht 2018). These techniques offer high-resolution imaging of subsurface features and can effectively delineate voids and weak zones. However, they are typically limited to relatively small areas (tens to hundreds of square meters) and are often deployed only after signs of ground deformation or structural damage have been observed due to their high cost and logistical constraints (Becker *et al.* 2024).

To overcome these limitations, satellite-based Interferometric Synthetic Aperture Radar (InSAR) has emerged as a powerful tool for ground deformation monitoring over large areas (Osmanoğlu *et al*. 2016). InSAR utilizes radar signals from Earth-orbiting satellites to measure ground surface movements with millimeter-level accuracy. This technique allows for the detection of localized deformation associated with sinkhole development across broad regions, providing valuable data that complements traditional geophysical and geotechnical surveys (Gutiérrez *et al.* 2011).

Numerous studies have successfully applied InSAR for sinkhole detection and subsidence monitoring worldwide, including in the Ebro Valley in Spain (Gutiérrez *et al.* 2011), the Dead Sea shores (Nof *et al*. 2019), Heerlen in the Netherlands (Chang and Hanssen, 2014), Gauteng province in South Africa (Theron *et al.* 2017), Texas, USA (Nur *et al*. 2024), Quebec City, Canada (Martel *et al.* 2018), and Prà di Lama in Italy (La Rosa *et al.* 2018).

An accurate sinkhole susceptibility assessment is crucial for mitigating the impact of sinkholes in Greene County. Sinkhole susceptibility mapping involves identifying areas more likely to experience sinkhole formation based on quantitative and qualitative analysis of various factors such as geology, hydrology, land use, topography, and historical sinkhole distribution (Zhang *et al*. 2024). Data-driven methods for sinkhole susceptibility mapping leverage advanced computational techniques and large datasets to predict areas at risk. Machine learning models, including Decision Tree (DT), Support Vector Machines (SVM), Logistic Regression (LR), Neural Networks, K-Nearest Neighbors (KNN), Random Forest (RF), and Gradient Boosting Decision Trees (GBDT), have been widely used to process extensive datasets and identify patterns associated with sinkhole occurrence *(Kim et al.* 2020, Nam *et al*. 2024, Zhang *et al*. 2024, Zhu *et al*. 2020). These models incorporate geomorphological factors derived from high-resolution elevation data, such as those obtained from Light Detection and Ranging (LiDAR) surveys, to enhance predictive capabilities. The performance of these models is typically evaluated using metrics like the Area Under the Curve (AUC) of the Receiver Operating Characteristic (ROC) curve, with higher AUC values indicating better predictive accuracy.

This study aims to integrate satellite-based InSAR data with machine learning techniques to improve sinkhole susceptibility mapping in Greene County, Missouri. We analyzed ground deformation using InSAR data from Sentinel-1 satellites for the period 2018 to 2020. A sinkhole inventory map was developed using unsupervised K-means clustering, and topographic conditioning factors were derived from LiDAR-based Digital Elevation Models (DEMs). An Artificial Neural Network (ANN) was employed to model sinkhole susceptibility, and the results were compared with the InSAR-derived deformation maps. Integrating InSAR data with advanced machine learning models aims to provide a comprehensive approach for detecting precursory subsidence and mapping zones susceptible to future sinkhole formation, thereby contributing to effective hazard mitigation and urban planning in karst regions.

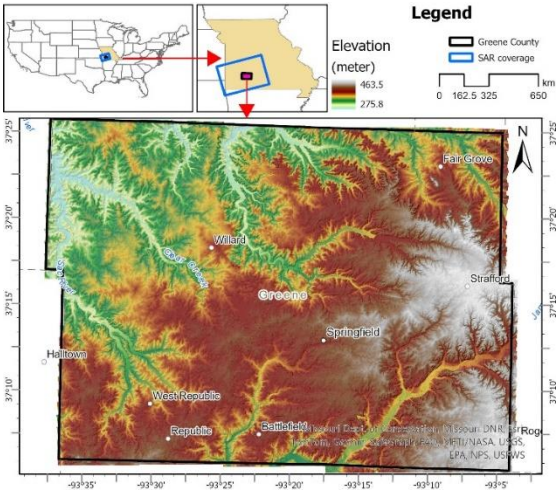

Fig. 1 Location of the study area in Greene County, Missouri, and Sentinel-1 satellite coverage (blue frame)

Fig. 2 Examples of active sinkholes in the study area.

2. Study area and datasets

2.1 Study area

Greene County, located in southwestern Missouri, spans from 37°5′20″ to 37°25′38″ N latitude and 93°3′51″ to 93°37′16″ W longitude (Fig. 1). Covering an area of approximately 1,756 square kilometers, it is the fourth most populous county in the state, home to about 300,000 residents. The county features a humid subtropical climate characterized by hot summers and cool winters. Precipitation is relatively consistent throughout the year, with a slight peak during the summer months due to frequent thunderstorms. The terrain elevation ranges from 27.8 meters to 473.5 meters above sea level, exhibiting varied topography that includes plateaus, rolling hills, and valleys.

Geologically, Greene County is underlain by thick sequences of well-karstified carbonate rocks, particularly

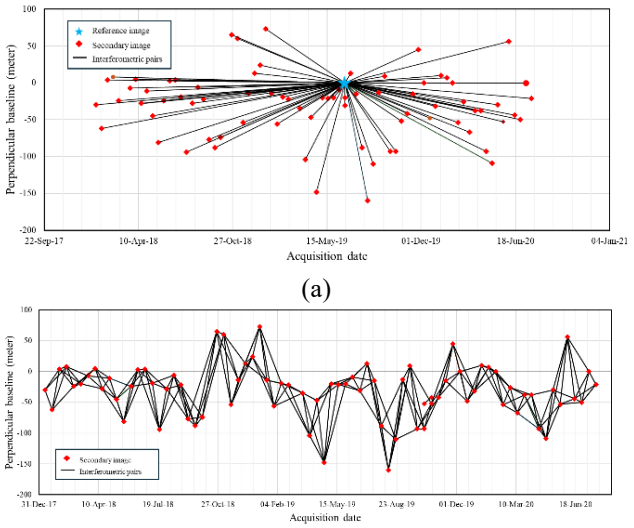

(a)

(b)

Fig. 3 Baseline plots used in (a) PSI and (b) SBAS processing. The blue star indicates the chosen reference image

the Mississippian-age Burlington-Keokuk Limestone (Kidanu *et al.* 2018). This limestone formation is known for its high solubility, making it susceptible to karst processes such as dissolution, which leads to the development of sinkholes, caverns, and springs (Tacim *et al.* 2023). The limestone strata contain chert nodules and are characterized by alternating layers of limestone and thin chert beds. The limestone has a coarse crystalline structure, is light gray in color, and consists primarily of nearly pure calcite. The uneven disintegration of the Burlington-Keokuk Limestone results in an extremely irregular bedrock-overburden interface, contributing to the complex subsurface conditions that facilitate sinkhole formation (Fellows 1970). Fig. 2 illustrates examples of active sinkholes observed within the study area.

The region's geology, combined with human activities such as urban development and land use changes, poses significant challenges related to ground stability and infrastructure safety. Understanding the spatial distribution of sinkholes and their underlying causes is essential for effective land management and hazard mitigation in Greene County.

2.2 Data sources

2.2.1 SAR datasets

For this study, we utilized Synthetic Aperture Radar (SAR) data acquired by the Sentinel-1 satellites operated by the European Space Agency (ESA). A total of 75 SAR scenes were collected in Interferometric Wide (IW) swath mode, covering the period from January 10, 2018, to July 22, 2020. The SAR data have a spatial resolution of approximately 5 meters by 20 meters and are acquired at a 34-degree incident angle. The data are of C-band frequency (with a wavelength of 5.6 cm) and were acquired in descending orbit over path number 63 and frame number 117 with vertical-vertical (VV) polarization.

The Sentinel-1 satellite constellation provides consistent and frequent coverage of the study area, making it suitable for monitoring ground deformation over time. The Sentinel-1 footprint, shown as a blue frame in Fig. 1, adequately encompasses the entire study area.

To facilitate the interferometric processing, we analyzed the temporal and perpendicular baseline configurations of the SAR data. Fig. 3(a) displays the baseline network for the Persistent Scatterer Interferometry (PSI) approach, where an optimal reference image dated June 22, 2019 (indicated by a blue star), was selected. Fig. 3(b) shows the interferometric pair network utilized in the Small BAseline Subset (SBAS) approach, with thresholds set at 36 days for the temporal baseline and 200 meters for the perpendicular baseline. These configurations ensure high coherence between interferometric pairs, which is critical for accurate ground deformation measurements.

2.2.2 GIS data and topographic factors

To develop the sinkhole susceptibility model, various geomorphometric factors were derived and incorporated as independent variables. The primary digital elevation data were obtained from the Copernicus Digital Elevation Model (DEM), which provides high-resolution elevation information. Using System for Automated Geoscientific Analyses (SAGA) Geographic Information System (GIS) software (http://saga-gis.org), we derived several topographic indices, which are commonly used to represent sinkhole-related factors in susceptibility modeling.

The geomorphometric indices include:

Aspect: Represents the orientation or azimuth of the slope, indicating the compass direction that the slope faces. Aspect influences microclimates by affecting factors such as solar radiation exposure, wind patterns, and precipitation distribution, which impact soil moisture and vegetation cover.

Convergence Index (CI): Measures the degree to which surface runoff converges or diverges over the terrain. Calculated based on the flow directions of adjacent cells, it helps identify areas where water accumulates (convergent zones) or disperses (divergent zones), influencing erosion and sediment deposition processes.

Mass Balance Index (MBI): Assesses the balance between erosion and deposition at a given location by considering transformed elevation, slope, and mean curvature. Positive values indicate areas of net deposition, while negative values denote net erosion, critical in understanding landscape stability.

Mid-Slope Position (MSP): Normalizes the slope position between ridges and valleys, ranging from 0 (valleys) to 1 (ridges). MSP helps identify relative slope positions, important in understanding geomorphological processes.

Multiresolution Ridge Top Flatness Index (MRRTF): Quantifies the flatness and elevation of ridge tops over multiple spatial scales. Higher values indicate flatter and higher elevation areas, generally more stable and less prone to erosion.

Multiresolution Index of Valley Bottom Flatness (MRVBF): Measures the flatness and relative lowness of

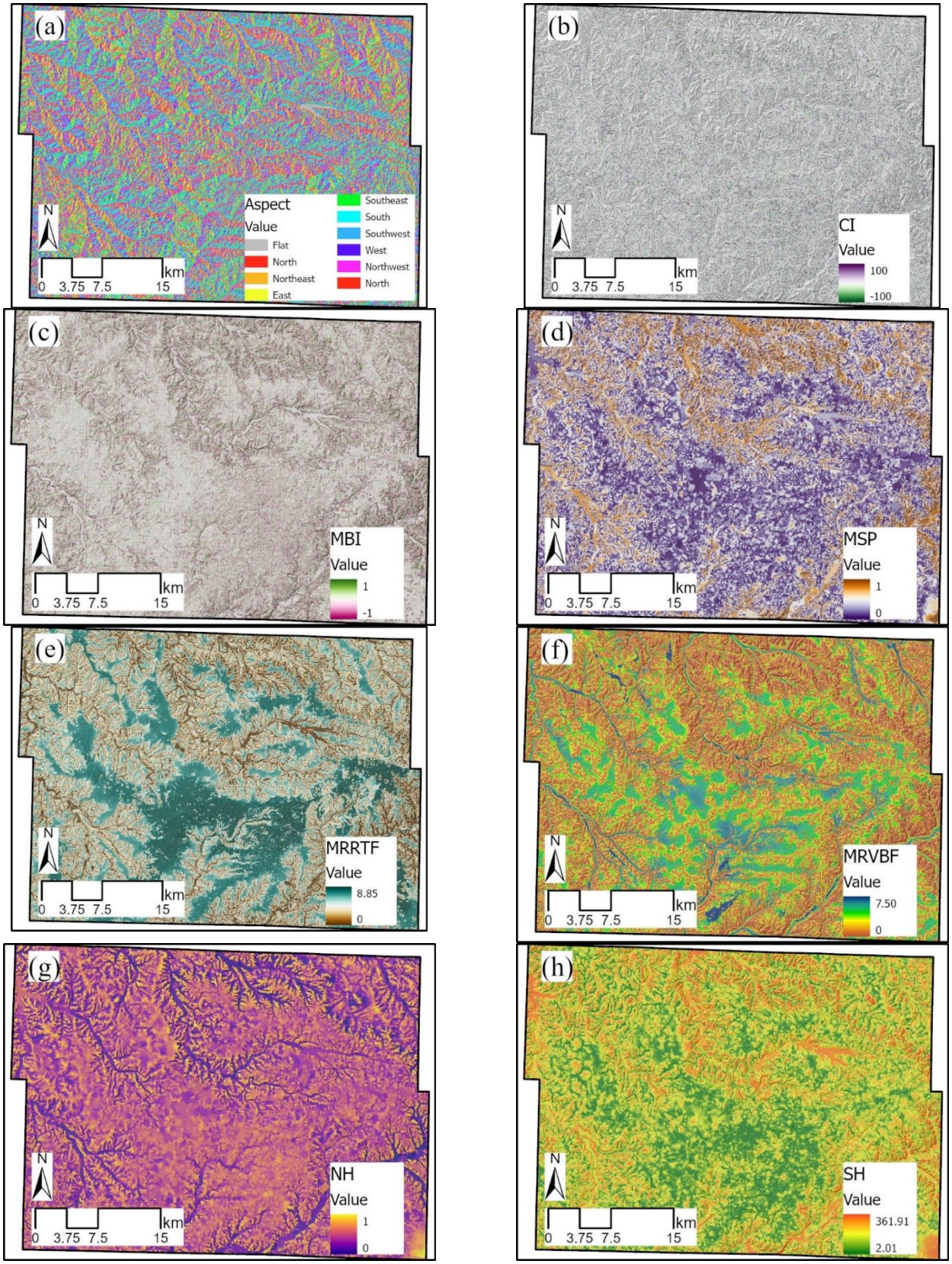

Fig. 4 Maps of geomorphometric factors: (a) aspect, (b) convergence index (CI), (c) mass balance index (MBI), (d) mid-slope position (MSP), (e) multiresolution ridge top flatness index (MRRTF), (f) multiresolution index of valley bottom flatness (MRVBF), (g) normal height (NH), (h) slope height (SH), (i) slope, (j) topographic position index (TPI), (k) topographic wetness index (TWI), and (l) land use

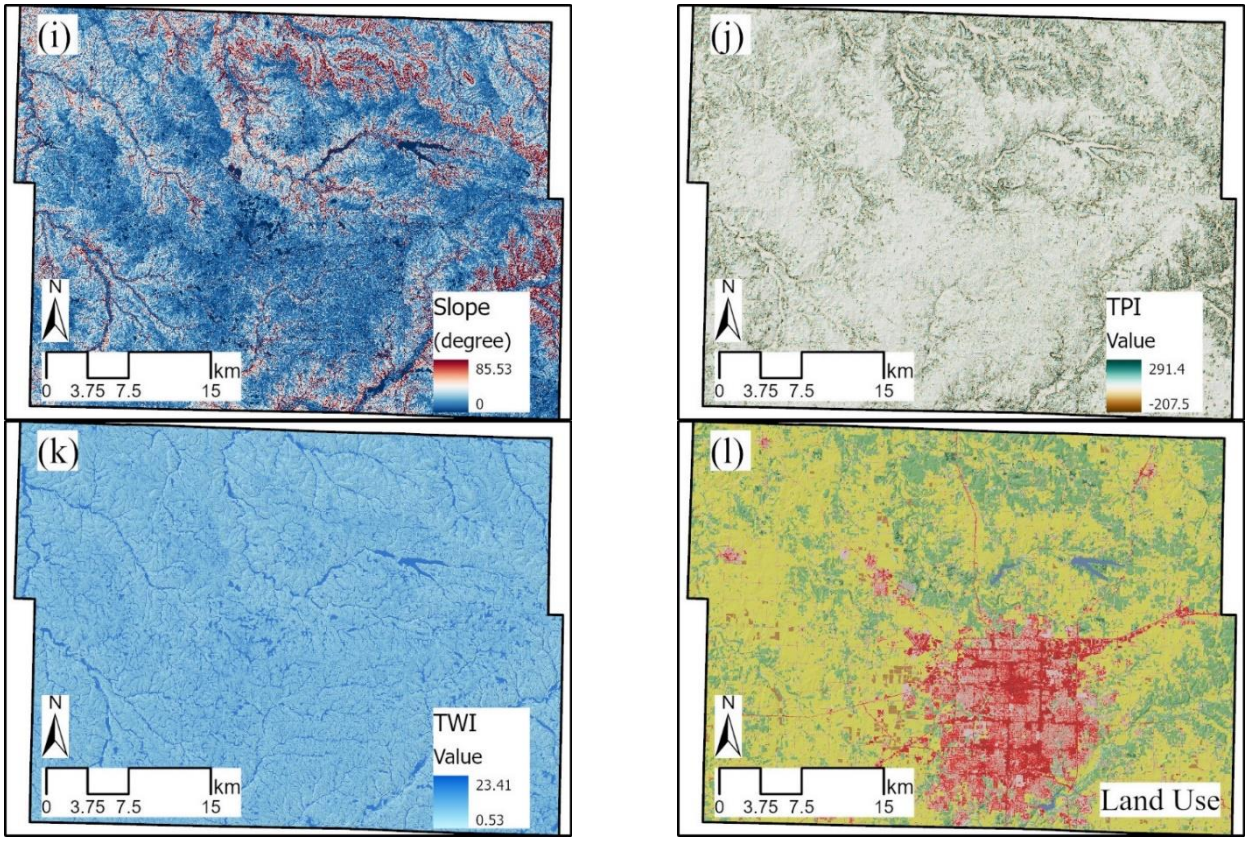

Fig. 4 Continued-

valley bottoms across multiple spatial resolutions. Higher values suggest broad, flat valley floors that can be areas of sediment accumulation and potential groundwater recharge.

Normal Height (NH): Represents the normalized elevation of a point relative to its surrounding terrain, providing insights into local topographic prominence or depression.

Slope Height (SH): Measures the vertical distance from a point to the nearest ridge or valley, providing a metric for relative elevation across the landscape.

Slope: Quantifies the steepness or gradient of the terrain, a critical factor in various geomorphological processes, including erosion, mass movements, and hydrological flow.

Topographic Position Index (TPI): Compares the elevation of a point to the mean elevation of its neighborhood, classifying the terrain into landform categories such as ridges, valleys, and flat areas.

Topographic Wetness Index (TWI): Combines local slope and upstream contributing area to estimate the potential for soil saturation and surface runoff, indicating areas prone to accumulation of moisture.

Additionally, land use data were incorporated to account for the influence of human activities and vegetation cover on sinkhole susceptibility. The land use data were obtained from satellite imagery and other relevant sources.

Initially, 15 geomorphometric indices were considered for the model development. However, during multicollinearity analysis and feature importance evaluation, three factors were excluded due to insignificance or high correlation with other variables, as detailed in Section 4.5. All raster datasets were standardized and resampled to a consistent spatial resolution of 30 meters to ensure compatibility within the GIS environment.

3. Methodology

3.1 InSAR processing

The study area encompasses both urban environments and surrounding agricultural regions, necessitating a comprehensive approach to ground deformation analysis. We employed a combination of PSI and SBAS InSAR techniques to leverage their respective strengths in capturing surface deformation over diverse land cover types (Osmanoğlu *et al.* 2016). The PSI method is particularly effective in densely built-up urban areas where numerous stable reflectors, such as buildings and infrastructure, provide coherent scatterers over time. PSI allows for high temporal resolution and precise monitoring of deformation at individual point locations (Ferretti *et al*. 2001). Conversely, the SBAS approach is well-suited for areas with distributed scatterers, such as natural terrains and agricultural fields, where coherence between SAR images can be maintained over shorter temporal baselines. SBAS utilizes multiple small baseline interferograms to retrieve deformation estimates over regions with varying coherence levels (Berardino *et al.* 2002).

By integrating PSI and SBAS methods, we aimed to achieve comprehensive spatial coverage and improve the reliability of ground deformation measurements across the entire study area. The combination enhances the density of measurement points by utilizing both persistent and distributed scatterers, allowing for continuous and detailed monitoring of surface deformation.

We utilized the open-source toolbox EZ-InSAR (easy-to-use InSAR), which integrates the InSAR Scientific Computing Environment (ISCE) and the Stanford Method for Persistent Scatterers (StaMPS) to generate interferograms and displacement time series (Hrysiewicz *et al.* 2023). EZ-InSAR streamlines the processing workflow by automating the download of Sentinel-1 SAR scenes and the necessary DEM data over the study area. The processing workflow is depicted in Fig. 5 and involves several key steps:

1. Data Acquisition: Sentinel-1 Single Look Complex (SLC) SAR data and precise orbit ephemeris files were downloaded for the study period. An external DEM, such as the Shuttle Radar Topography Mission (SRTM) DEM, was also obtained to assist in phase calculations.
2. Data Preparation and Coregistration: SAR images were coregistered to a common master image to ensure precise alignment of pixels across the dataset, critical for accurate interferometric analysis. For the PSI approach, a single reference scene dated June 22, 2019, was selected based on spatial and temporal criteria (Fig. 3(a)). For the SBAS approach, multiple interferometric pairs were formed using thresholds of 36 days for temporal baselines and 200 meters for perpendicular baselines to maintain coherence (Fig. 3(b)).
3. Interferogram Generation: Interferograms were generated by computing the phase differences between coregistered SAR image pairs. The orbital parameters and DEM data were used to remove topographic phase contributions and calculate the differential interferometric phase related to surface deformation.
4. Phase Unwrapping and Time-Series Analysis: The wrapped interferometric phases were unwrapped to retrieve the actual phase differences. The StaMPS algorithm was employed to perform time-series analysis for both PSI and SBAS methods, estimating the line-of-sight (LOS) displacement time series for each coherent pixel.
5. Atmospheric Corrections and Error Mitigation: Atmospheric phase screen (APS) estimates were computed and removed to reduce atmospheric artifacts in the displacement measurements. Noise reduction techniques were applied to enhance the signal-to-noise ratio and improve the accuracy of the deformation estimates.
6. Integration of PSI and SBAS Results: The displacement time series and mean deformation rates from the PSI and SBAS analyses were merged to enhance the spatial density of measurement points and to provide a comprehensive deformation map covering both urban and rural areas.

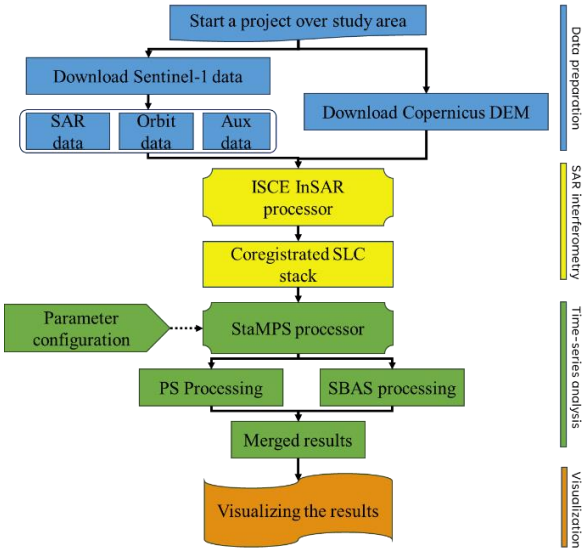

Fig. 5 InSAR processing workflow using EZ-InSAR

The combined use of PSI and SBAS methods, facilitated by the EZ-InSAR toolbox, enabled us to detect minute ground movements and to monitor temporal changes in surface deformation associated with karst processes and sinkhole development.

3.2 Unsupervised clustering for sinkhole inventory

To prepare a comprehensive sinkhole inventory for the study area, we applied an unsupervised clustering algorithm to identify and categorize sinkhole features based on their spatial characteristics. Unsupervised clustering algorithms facilitate the self-organization of data without prior knowledge of the categories of any objects (Kassambara 2017). They enhance understanding by identifying similar patterns within the data and grouping each object accordingly.

We employed the K-means clustering algorithm, which partitions the dataset into a predefined number of clusters (k) by minimizing the within-cluster sum of squares (WCSS) (MacQueen 1967). The K-means algorithm minimizes the sum of squared distances between data points and their respective cluster centroids, aiming to achieve compact and well-separated clusters.

Mathematically, the objective function that K-means minimizes is defined as:

$$J = \sum_{j=1}^{k} \sum_{i=1}^{n_j} \left\| x_i^{(j)} - c_j \right\|^2 \quad (1)$$

where J is the total WCSS, k is the number of clusters, n_j is the number of data points in cluster j, k is the total number of clusters, $x_i^{(j)}$ is the i-th data point assigned to cluster j, c_j is the centroid of cluster j, and $\|\cdot\|$ denotes the Euclidean distance.

The K-means algorithm operates iteratively, performing the following steps until convergence:

1. Initial Centroid Selection: Randomly select k initial centroids.
2. Cluster Assignment: Assign each data point to the

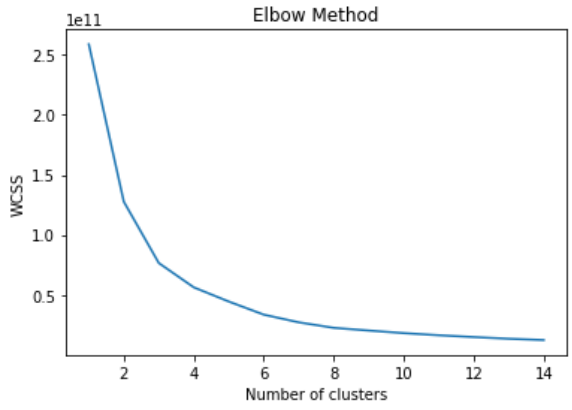

(a)

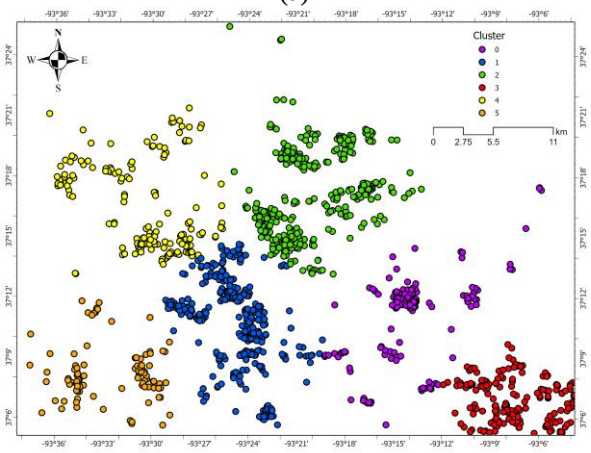

(b)

Fig. 6 (a) Elbow method for determining the optimal number of clusters. (b) Spatial distribution of sinkhole clusters identified using K-means algorithm

nearest centroid based on Euclidean distance.

3. Centroid Update: Recalculate the centroids by computing the mean of all data points assigned to each cluster.
4. Convergence Check: Repeat steps 2 and 3 until the centroids no longer change significantly or a maximum number of iterations is reached.

The optimal number of clusters (k) was determined using the Elbow Method, which involves plotting the WCSS against different values of k to identify a point where increasing the number of clusters yields diminishing returns in terms of reducing WCSS (Fig. 6(a)). The Elbow Method suggested an optimal value of k = 6, balancing the trade-off between model complexity and explanatory power.

By clustering the sinkhole data, we categorized the sinkholes based on spatial proximity and morphological characteristics, which facilitated the subsequent analysis and modeling of sinkhole susceptibility. The clustering results are illustrated in Fig. 6(b).

3.3 Sinkhole susceptibility mapping

Sinkhole susceptibility mapping assesses the probability of sinkhole occurrence in a specific geographical area based on various environmental factors. The process aims to delineate zones with varying levels of susceptibility to guide land use planning and hazard mitigation efforts.

We developed the sinkhole susceptibility map using a machine learning approach, specifically an Artificial Neural Network (ANN), which is well-suited for modeling complex, non-linear relationships between input variables and target outcomes (Wang 2003). The modeling process consisted of several key steps (Fig. 6):

- Data Preparation: We compiled a sinkhole inventory map based on data from the Geological Survey Program of the Missouri Department of Natural Resources (MoDNR), which documented approximately 1,303 sinkholes in the study area as of December 2018. Additional sinkholes identified through clustering and analysis of landform features were incorporated into the inventory.
- Selection of Conditioning Factors: The geomorphometric indices and land use data described in Section 2.2.2 were prepared as independent variables in the model. These factors represent the environmental parameters that influence sinkhole formation.
- Training and Testing Datasets: The sinkhole inventory was randomly divided into training and testing datasets, with 70% of the points used to train the ANN model and the remaining 30% reserved for model validation. This partitioning follows best practices in machine learning to prevent overfitting and to assess the model's generalization capability (Fadhillah *et al*. 2022, Hakim *et al.* 2023).
- Modeling with Artificial Neural Networks: The ANN model was constructed using a Multilayer Perceptron (MLP) architecture, consisting of an input layer, one or more hidden layers, and an output layer. Input nodes corresponded to the conditioning factors, and the output node represented the sinkhole susceptibility score. The network parameters, including the number of hidden layers and neurons, activation functions, and learning rate, were optimized through cross-validation.
- Model Evaluation and Validation: The performance of the ANN model was evaluated using the testing dataset. Metrics such as the ROC curve and the AUC value were computed to assess the model's predictive accuracy (Luat *et al*. 2024). A high AUC value indicates that the model effectively discriminates between areas with and without sinkhole occurrences.
- Generation of Sinkhole Susceptibility Map: The trained ANN model was applied to the entire study area, producing a continuous sinkhole susceptibility score for each pixel. The susceptibility scores were classified into five categories (very low, low, moderate, high, and very high) using the natural breaks classification method, which identifies natural groupings in the data (Hakim *et al*. 2022).
- Analysis of Factor Importance: To identify the most influential factors in the model, Mutual Information

(MI) analysis was conducted. MI quantifies the amount of information shared between input features and the target variable, helping to determine which factors contribute most to the prediction of sinkhole susceptibility.

3.4 Artificial Neural Network framework

Artificial Neural Networks (ANNs) are computational models inspired by the biological neural networks of the human brain. ANNs are capable of modeling complex, non-linear relationships between input and output variables by learning from data (Wang, 2003).The MLP is a widely used feedforward ANN architecture, consisting of an input layer, one or more hidden layers, and an output layer (Günther and Fritsch 2010).

In our sinkhole susceptibility modeling, the MLP architecture was employed with the following considerations:

- Input Layer: Consisted of 12 neurons corresponding to the selected conditioning factors (e.g., aspect, slope, TPI, MRVBF).
- Hidden Layers: Included one or more hidden layers to capture the non-linear interactions among the input variables. The number of neurons in each hidden layer was determined through experimentation and cross-validation to balance model complexity and performance. Here, 32 nodes are the optimal number of neurons.
- Activation Functions: Used non-linear activation functions, which is rectified linear unit (ReLU), to introduce non-linearity into the model, enabling it to learn complex patterns.
- Output Layer: Comprised a single neuron producing a sinkhole susceptibility score, a continuous value representing the likelihood of sinkhole occurrence.
- Training Process: Employed a supervised learning approach, minimizing a loss function (e.g., mean squared error) through the Adam optimizer, with learning rate of 0.01.
- Weight Initialization and Regularization: Applied proper initialization of weights and incorporation of regularization techniques (e.g., L1 or L2 regularization, dropout) to prevent overfitting and enhance the model's generalization capability.

The mathematical representation of the MLP is given by

$$y = f\left(\sum_{i=1}^{n} w_i x_i + b\right) \quad (2)$$

where y is the output, x_i are the input features, w_i are the weights, b is the bias term, and $f(\cdot)$ is the activation function. The number of epochs was set to 2000, and the RMSE value used for the stopping criterion was set to 0.01. All the iterations met the 0.01 root mean square error goal in less than 2000 epochs.

The ANN model was implemented using machine learning libraries such as TensorFlow or scikit-learn (Pedregosa *et al.* 2011), allowing for efficient computation and model tuning. The model's predictive performance was rigorously evaluated to ensure its suitability for sinkhole susceptibility mapping.

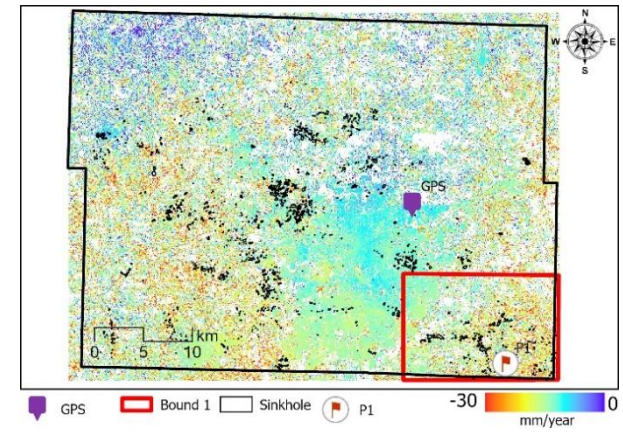

(a)

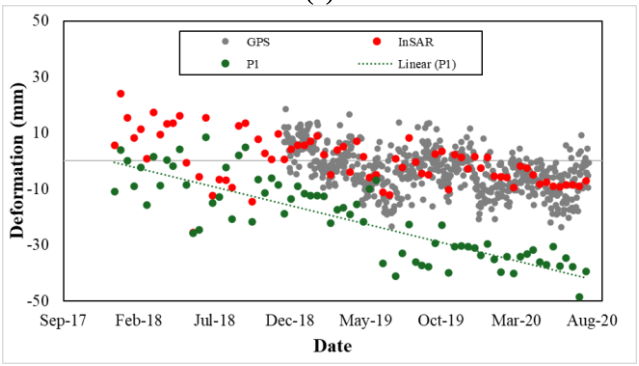

(b)

Fig. 7 (a) Mean deformation rate map from PSI and SBAS analysis. (b) Comparison between GPS and InSAR measurements

4. Results and discussion

4.1 Ground deformation analysis using InSAR

The combined PSI and SBAS analysis provided detailed insights into ground surface deformation in Greene County over the study period from January 2018 to July 2020. The mean deformation rate map, shown in Fig. 7(a), illustrates the spatial distribution of ground displacement along the satellite's LOS. The deformation rates range from negligible movements to subsidence reaching up to 30 millimeters per year.

The deformation patterns indicate that the most significant subsidence occurs in urban areas as well as in adjacent agricultural regions. These areas coincide with zones underlain by karstified carbonate rocks, suggesting a strong link between subsurface karst processes and observed ground movements.

To validate the InSAR-derived deformation measurements, we compared the time-series data with continuous global positioning system (GPS) observations from a nearby continuously operating reference station (CORS) maintained by the National Geodetic Survey (NGS). The comparison, depicted in Fig. 7(b), demonstrates a reasonable agreement between the InSAR and GPS measurements, with a root mean square error (RMSE) of approximately 8.5 mm/year. Discrepancies may be attributed to local site effects (soil type, roughness, vegetation or urban structures), atmospheric disturbances (water vapor and change in pressure), or

differences in the spatial resolution and observation geometries of the two measurement techniques (Ding *et al.* 2008, Hakim *et al.* 2023).

Furthermore, we analyzed the temporal evolution of deformation at specific points of interest, such as Point 1 located over an identified sinkhole. The time-series plot at this location indicates cumulative subsidence of up to 50 millimeters over the study period, highlighting the capability of InSAR techniques to detect and monitor subtle ground movements associated with sinkhole development.

This study is limited by the use of Sentinel-1 SAR data with a 30-meter resolution, which restricts its ability to detect surface deformations caused by small sinkholes. From the 2023 sinkhole data, approximately 3,000 sinkholes have an area smaller than 1,000 m², making it challenging for InSAR to identify newly formed sinkholes, especially those below this size threshold. The spatial resolution of the satellite data significantly impacts the effectiveness of sinkhole monitoring, and higher-resolution satellites such as TerraSAR-X (0.3m) or COSMO-SkyMed (0.5 m) could serve as alternatives for capturing finer-scale surface deformations. Future studies may benefit from integrating these high-resolution datasets to improve sinkhole detection and monitoring accuracy.

4.2 Sinkhole inventory and clustering analysis

To enhance the sinkhole inventory and facilitate the susceptibility modeling, we performed a clustering analysis using the K-means algorithm. The optimal number of clusters was determined to be 6 based on the Elbow method (Fig. 6(a)), which balances model simplicity with explanatory power. Increasing the number of clusters beyond 6 resulted in minimal reductions in WCSS, indicating diminishing returns in model performance.

The clustering results, presented in Fig. 6(b), group the sinkholes into distinct clusters based on spatial proximity and morphological characteristics. These clusters indicate non-random sinkhole distribution, likely influenced by geological, hydrological, or environmental factors. Higher-density clusters (e.g., red) suggest areas with more susceptible subsurface conditions, while more dispersed clusters (e.g., orange) may indicate varied formation processes. This categorization aids in understanding regional patterns of sinkhole occurrence and supports the stratification of data for modeling purposes.

The K-means clustering algorithm, while, simple to implement, efficient and widely used, has several limitations when applied to sinkhole inventory datasets. It assumes clusters are spherical and of similar density, which may not reflect the irregular and varied spatial distribution of sinkholes. Additionally, K-means requires the number of clusters (K) to be predefined, struggles with outliers, and is sensitive to initialization, potentially leading to inconsistent results. Given these limitations, alternative clustering techniques may be more suitable. Density Based Spatial Clustering of Applications with Noise (DBSCAN), for instance, is effective for detecting arbitrarily shaped clusters and handling noise, making it useful for sinkhole detection in complex geological settings (Kumar and Reddy 2016). Hierarchical clustering provides insights into nested relationships without requiring a predefined K, while Gaussian Mixture Models (GMM) allow for cluster overlap, accommodating the uncertainty in sinkhole boundaries (Wang *et al.* 2019). However, when we tested several alternative clustering methods, including Affinity Propagation, Agglomerative, Balanced Iterative Reducing and Clustering using Hierarchies (BIRCH), and Mini Batch K-means Clustering, the results showed very similar cluster patterns. This suggests that the distribution of sinkholes in our study area is quite efficiently represented by the K-means method, without requiring the more complicated techniques. Given this, K-means proves to be an effective and computationally efficient choice for clustering sinkholes, as it accurately captures the spatial distribution of sinkholes in the area without the need for more complex methods.

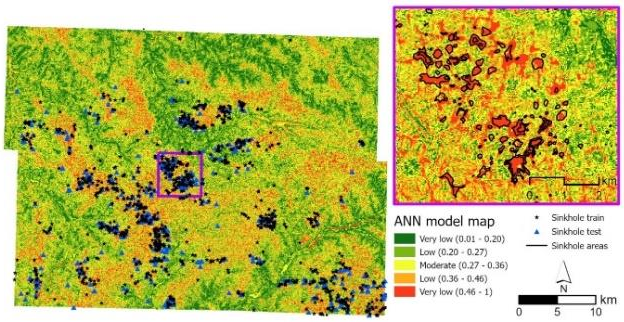

Fig. 8 Sinkhole susceptibility map of Greene County

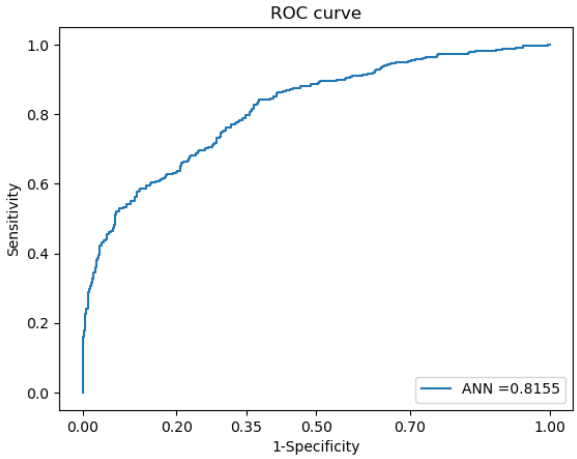

Fig. 9 The ROC curve and AUC value of ANN model for sinkhole susceptibility mapping

4.3 Sinkhole susceptibility mapping

The sinkhole susceptibility map generated using the ANN model is shown in Fig. 8. Each pixel in the study area was assigned a sinkhole susceptibility score, which was categorized into five classes—very low, low, moderate, high, and very high—using the natural break classification method. This method effectively groups similar susceptibility values and maximizes the differences between classes, enhancing the interpretability of the map.

The map reveals that approximately 30% of the study area is classified as having very high sinkhole susceptibility. These

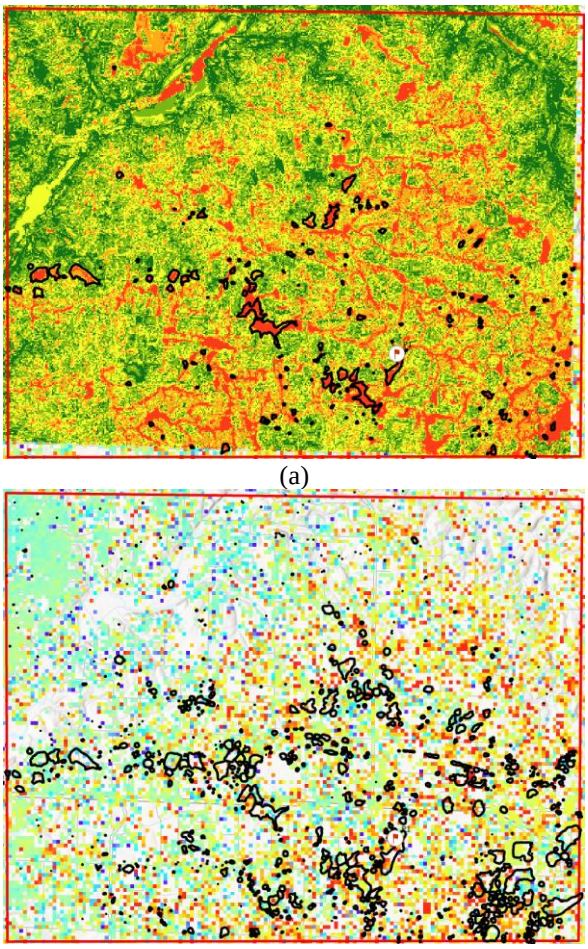

(a) (b)

Fig. 10 (a) Susceptibility map with 2018 sinkhole data and (b) Deformation map with 2023 sinkhole data.

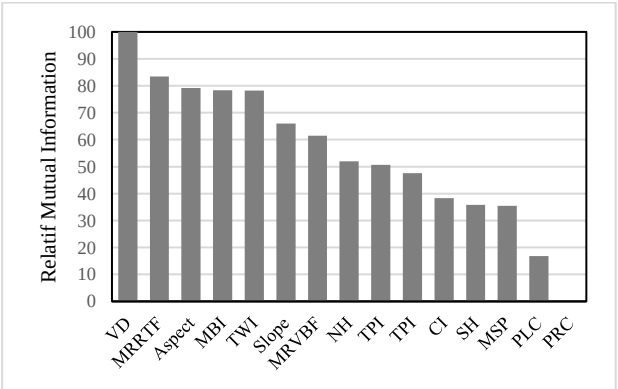

Fig. 11 Mutual information scores of conditioning factors.

areas are predominantly located in the central, southwestern, and southeastern parts of Greene County. The high susceptibility zones are characterized by specific geomorphometric conditions, including high values of MRRTF and TWI, coupled with gentle slopes. These factors contribute to conditions favorable for sinkhole development, such as increased infiltration and subsurface dissolution of carbonate rocks.

Another 30% of the area exhibits moderate sinkhole susceptibility, while the remaining 40% is classified as having low to very low susceptibility. The low susceptibility zones are associated with high values of MBI and MSP, indicating areas with less favorable conditions for sinkhole formation.

The ANN model's predictive performance was evaluated using the testing dataset and ROC curve analysis with AUC value of 0.8155 (Fig. 9), demonstrating a high level of accuracy in distinguishing between sinkhole and non-sinkhole areas. The detailed analysis of the susceptibility map supports its utility in planning and hazard mitigation efforts.

4.4 Correlation between subsidence and sinkhole occurrence

An intriguing observation arises when comparing the sinkhole susceptibility map with the recent sinkhole inventory data released by MoDNR in 2023. The updated inventory reports a significant increase in the number of documented sinkholes, totaling 7,541—a substantial rise of 6,238 sinkholes since 2018. This dramatic increase underscores the growing concern over sinkhole hazards in the region.

Notably, many of the newly identified sinkholes overlap with areas exhibiting significant subsidence as detected by the InSAR analysis, particularly in regions highlighted by the red box in Fig. 9. This spatial correlation suggests a strong linkage between ground subsidence and the occurrence of sinkholes, reinforcing the validity of the InSAR-derived deformation patterns.

Furthermore, the ANN-based sinkhole susceptibility map shows high potential sinkhole areas that correspond with the locations of new sinkholes identified in the 2023 inventory (Fig. 10(a)). This correspondence indicates the predictive capability of the ANN model in forecasting areas prone to future sinkhole development.

Table 1 VIF and TOL scores for conditioning factors

No	Factors	VIF	TOL
1	Aspect	1.19	0.84
2	CI	1.94	0.52
3	LU	2.12	0.47
4	MBI	2.71	0.37
5	MSP	1.51	0.66
6	MRRTF	2.04	0.49
7	MRVBF	2.59	0.39
8	NH	2.51	0.40
9	PLC	1.87	0.53
10	PRC	1.49	0.67
11	SH	2.48	0.40
12	Slope	4.33	0.23
13	TPI	3.39	0.29
14	TWI	3.53	0.28
15	VD	767.02	0.001

An example of significant concern is the sinkhole labeled as P1, which expanded from an area of 118,033 square meters in 2018 to an alarming 295,110 square meters in 2023. The rapid expansion of existing sinkholes and the emergence of new ones highlight the dynamic nature of karst processes in the karst-prone region and the importance of continuous monitoring.

The InSAR results showing surface deformation indicated by yellow to red pixels correspond with new sinkholes location and very high sinkhole susceptible areas (Fig. 10(b)). These results show the capability of InSAR to detect sinkhole occurrence on karst-prone region, similar to other studies such as sinkhole monitoring in Elba Island, Italy using GB-InSAR (Intrieri *et al*. 2015), kerdabad, Iran using PS-InSAR method (Khoshlahjeh Azar *et al.* 2021). These findings demonstrate the effectiveness of integrating InSAR deformation analysis with sinkhole susceptibility modeling to identify and monitor areas at risk. The combined approach provides valuable information for proactive management and mitigation strategies to address sinkhole hazards.

4.5 Analysis of factor importance

To assess the relative importance of the conditioning factors in the sinkhole susceptibility model, we employed MI analysis. MI quantifies the dependency between input variables and the target outcome, with higher MI values indicating stronger predictive power (Ross 2014).

The MI results, presented in Fig. 11, reveal that the Valley Depth (VD) factor has the highest MI score, indicating it is the most informative predictor of sinkhole occurrence. This is followed by the Multiresolution Ridge Top Flatness Index (MRRTF), aspect, and Mass Balance Index (MBI).

Conversely, factors such as Profile Curvature (PRC) and Plan Curvature (PLC) showed low MI scores, suggesting they contribute less to distinguishing between sinkhole and non-sinkhole areas. Additionally, multicollinearity analysis was conducted using the Variance Inflation Factor (VIF) and tolerance (TOL) metrics to identify redundant variables. Factors with VIF scores exceeding 10 and TOL values below 0.1 indicate high multicollinearity and were considered for exclusion (Table 1).

Based on these analyses, factors such as VD, PLC, and PRC were excluded from the final modeling process due to redundancy or insignificance. Exclusion of these factors improved the robustness of the model by reducing overfitting and enhancing predictive accuracy.

This systematic evaluation ensures that the most influential and independent factors are included in the sinkhole susceptibility model, optimizing its performance and reliability. While this study provides valuable insights into sinkhole formation and risk assessment, future study needs to consider critical environmental and geological factors such as soil properties, groundwater flow dynamics, and anthropogenic influences. Furthermore, while climate change plays a significant role in sinkhole formation, this study does not comprehensively assess the effects of changing precipitation patterns and extreme weather events, which should be a focus of future research to improve long-term risk assessment and mitigation strategies.

5. Conclusions

In this study, we conducted a comprehensive assessment of ground deformation and sinkhole susceptibility in Greene County, Missouri, by integrating satellite-based InSAR techniques with advanced machine learning models. The combination of PSI and SBAS methods enabled us to detect and monitor ground surface deformation across both urban and rural areas with high spatial resolution. The InSAR analysis revealed significant subsidence in the study area, with deformation rates reaching up to 30 millimeters per year along the satellite's LOS. These high deformation zones correspond closely with regions underlain by karstified carbonate rocks, indicating active subsurface karst processes.

The deformation time series derived from InSAR was validated against continuous GPS measurements, yielding an RMSE of approximately 8.5 mm/year. This validation confirms the reliability of the InSAR results, although discrepancies due to local site conditions and atmospheric effects were noted.

Using an ANN model, we developed a sinkhole susceptibility map incorporating geomorphometric factors derived from high-resolution LiDAR data. The model classified approximately 30% of the study area as highly susceptible to sinkhole formation, aligning with areas exhibiting significant ground deformation. The ANN model demonstrated strong predictive capability, evidenced by its ability to identify regions where new sinkholes have emerged, according to the updated sinkhole inventory data from 2023.

Statistical analyses, including MI and multicollinearity evaluations, identified key conditioning factors significantly influencing sinkhole susceptibility. Factors such as MRRTF, aspect, and MBI were recognized as the most important predictors. Conversely, factors exhibiting high redundancy or multicollinearity were excluded to enhance model robustness.

Integrating InSAR data with machine learning techniques provides a powerful approach for detecting subtle ground movements and predicting areas at risk of sinkhole development. This methodology offers valuable insights for land use planning, infrastructure development, and hazard mitigation in karst regions.

Future research should focus on refining the predictive models by incorporating additional environmental and geological factors, such as soil properties, groundwater flow dynamics, and anthropogenic influences. Additionally, assessing the impacts of climate change, particularly changes in precipitation patterns and extreme weather events, on sinkhole formation is essential for long-term risk assessment. The framework can incorporate time-series data on groundwater flow, precipitation trends, and soil moisture variations. Groundwater fluctuations, influenced by prolonged droughts or excessive rainfall, directly impact the stability of underground voids. By integrating hydrological models and remote sensing data, future study can refine sinkhole susceptibility predictions based on real-time environmental

changes.

Overall, this study contributes a valuable framework for regional planning and hazard mitigation, supporting proactive management strategies to address subsidence and sinkhole risks in karst landscapes like Greene County, Missouri.

Acknowledgments

The authors would like to acknowledge the support provided by the Missouri Department of Natural Resources for supplying sinkhole inventory data. We also express our gratitude to the European Space Agency (ESA) for providing the Sentinel-1 SAR data used in this study. Special thanks go to the National Geodetic Survey (NGS) for the GPS data used in validation.

References

Abdelmawla, A., Ma, S., Yang, J.J. and Kim, S.S. (2023), "Subsurface anomaly detection utilizing synthetic GPR images and deep learning model", *Geomech. Eng*., **33**(2), 203-209. https://doi.org/10.12989/gae.2023.33.2.203.

Barner, W. and Gouzie, D. (2024), "Urbanization in a karst terrane, Springfield, Missouri, USA. In Field Guides to the Ozarks: Exploring Karst, Ore, Trace Fossils, and Orogenesis", 1-17. Geological Society of America. https://doi.org/10.1130/2024.0068(01).

Becker, D., Raddatz, L., Roussel, C. and Klonowski, J. (2024), "Analysis methods for deformation detection using TLS and UAS data on the example of a landslide simulation", *Int. J. Geo-Eng.*, **15**(1), 9. https://doi.org/10.1186/s40703-023-00203-z.

Berardino, P., Fornaro, G., Lanari, R. and Sansosti, E. (2002), "A new algorithm for surface deformation monitoring based on small baseline differential SAR interferograms", *IEEE T. Geosci. Remote Sens*., **40**(11), 2375-2383. https://doi.org/10.1109/TGRS.2002.803792.

Chang, L. and Hanssen, R.F. (2014), "Detection of cavity migration and sinkhole risk using radar interferometric time series", *Remote Sens. Environ*., **147**, 56-64. https://doi.org/10.1016/j.rse.2014.03.002.

Min, D.H. and Yoon, H.K. (2024), "Application of Ground Penetrating Radar (GPR) coupled with Convolutional Neural Network (CNN) for characterizing underground conditions", *Geomech. Eng*., **37**(5), 467-474. https://doi.org/10.12989/gae.2024.37.5.467.

Ding, X., Li, Z., Zhu, J., Feng, G. and Long, J. (2008), "Atmospheric effects on InSAR measurements and their mitigation". *Sensors*, **8**(9), 5426-5448. https://doi.org/10.3390/s8095426.

Fadhillah, M.F., Hakim, W.L., Panahi, M., Rezaie, F., Lee, C.W. and Lee, S. (2022), "Mapping of landslide potential in Pyeongchang-gun, South Korea, using machine learning meta-based optimization algorithms", *Egyptian J. Remote Sens. Sp. Sci.*, **25**(2), 463-472. https://doi.org/10.1016/j.ejrs.2022.03.008.

Fellows, L.D. (1970), "Geology of the galloway quadrangle, greene county, Missouri", Missouri Geological Survey and Water Resources.

Ferretti, A., Prati, C. and Rocca, F. (2001). "Permanent scatterers in SAR interferometry", *IEEE T. Geosci. Remote Sens*., **39**(1), 8-20. https://doi.org/10.1109/36.898661.

Günther, F. and Fritsch, S. (2010), "Neuralnet: training of neural networks", *R J*., **2**(1), 30.

Gutiérrez, F., Galve, J.P., Lucha, P., Castañeda, C., Bonachea, J. and Guerrero, J. (2011), "Integrating geomorphological mapping, trenching, InSAR and GPR for the identification and characterization of sinkholes: A review and application in the mantled evaporite karst of the Ebro Valley (NE Spain)", *Geomorphology*, **134**(1-2), 144-156. https://doi.org/10.1016/j.geomorph.2011.01.018.

Hakim, W.L., Fadhillah, M.F., Park, S., Pradhan, B., Won, J.S. and Lee, C.W. (2023), "InSAR time-series analysis and susceptibility mapping for land subsidence in Semarang, Indonesia using convolutional neural network and support vector regression", *Remote Sens. Environ*., **287**, 113453. https://doi.org/10.1016/j.rse.2023.113453.

Hakim, W.L., Rezaie, F., Nur, A.S., Panahi, M., Khosravi, K., Lee, C.W. and Lee, S. (2022), "Convolutional neural network (CNN) with metaheuristic optimization algorithms for landslide susceptibility mapping in Icheon, South Korea", *J. Environ. Management*, **305**, 114367. https://doi.org/10.1016/J.JENVMAN.2021.114367.

Han, J., Nur, A., Syifa, M., Ha, M., Lee, C.W. and Lee, K.Y. (2021). "Improvement of earthquake risk awareness and seismic literacy of Korean citizens through earthquake vulnerability map from the 2017 Pohang earthquake, South Korea", *Remote Sens*., **13**(7), 1365. https://doi.org/10.3390/rs13071365.

Hooper, A.J. (2008), "A multi-temporal InSAR method incorporating both persistent scatterer and small baseline approaches", *Geophys. Res. Lett*., **35**(16). https://doi.org/10.1029/2008GL034654.

Hooper, A., Zebker, H., Segall, P. and Kampes, B. (2004), "A new method for measuring deformation on volcanoes and other natural terrains using InSAR persistent scatterers", *Geophys. Res. Lett*., **31**(23), 1-5. https://doi.org/10.1029/2004GL021737.

Hrysiewicz, A., Wang, X. and Holohan, E.P. (2023), "EZ-InSAR: "An easy-to-use open-source toolbox for mapping ground surface deformation using satellite interferometric synthetic aperture radar", *Earth Sci. Inform*., **16**(2), 1929-1945. https://doi.org/10.1007/s12145-023-00973-1.

Intrieri, E., Gigli, G., Nocentini, M., Lombardi, L., Mugnai, F., Fidolini, F. and Casagli, N. (2015), "Sinkhole monitoring and early warning: An experimental and successful GB-InSAR application", *Geomorphology*, **241**, 304-314. https://doi.org/10.1016/j.geomorph.2015.04.018.

Kassambara, A. (2017), "Practical guide to cluster analysis in R: Unsupervised machine learning", (Vol. 1). Sthda.

Khoshlahjeh Azar, M., Hamedpour, A., Maghsoudi, Y. and Perissin, D. (2021), "Analysis of the deformation behavior and sinkhole risk in Kerdabad, Iran using the PS-InSAR method", *Remote Sens.*, **13**(14), 2696. https://doi.org/10.3390/rs13142696.

Kidanu, S.T., Anderson, N.L. and Rogers, J.D. (2018), "Using GIS-based spatial analysis to determine factors influencing the formation of sinkholes in greene county, Missouri".

Kim, Y.J., Nam, B.H., Jung, Y.H., Liu, X., Choi, S., Kim, D. and Kim, S. (2022). "Probabilistic spatial susceptibility modeling of carbonate karst sinkhole", Eng. Geol., **306**, 106728. https://doi.org/10.1016/j.enggeo.2022.106728.

Kim, Y.J., Nam, B.H., Shamet, R., Soliman, M. and Youn, H. (2020), "Development of sinkhole susceptibility map of east central Florida", *Nat. Hazard. Review*, **21**(4). https://doi.org/10.1061/(ASCE)NH.1527-6996.0000404.

Kumar, M.K. and Reddy, A.R.M. (2016), "A fast DBSCAN clustering algorithm by accelerating neighbor searching using Groups method", *Pattern Recogn.*, **58**, 39-48. https://doi.org/10.1016/j.patcog.2016.03.008.

La Rosa, A., Pagli, C., Molli, G., Casu, F., De Luca, C., Pieroni, A., and D'Amato Avanzi, G. (2018), "Growth of a sinkhole in a seismic zone of the northern Apennines (Italy)", *Nat. Hazards Earth Syst. Sci*., **18**(9), 2355-2366. https://doi.org/10.5194/nhess-18-2355-2018.

Luat, N.V., Do, T.N., Nguyen, L.C. and Kien, N.T. (2024), "Assessing landslide susceptibility along the Halong–Vandon expressway in Quang Ninh province, Vietnam: A comprehensive approach integrating GIS and various methods", *Geomech. Eng.*, **37**(2), 135-147. https://doi.org/10.12989/gae.2024.37.2.135.

MacQueen, J. (1967), "Some methods for classification and analysis of multivariate observations", *Proceedings of the 5th Berkeley Symposium on Mathematical Statistics and Probability/University of California Press*.

Martel, R., Castellazzi, P., Gloaguen, E., Trépanier, L. and Garfias, J. (2018), "ERT, GPR, InSAR, and tracer tests to characterize karst aquifer systems under urban areas: The case of Quebec City", *Geomorphology*, **310**, 45-56. https://doi.org/10.1016/j.geomorph.2018.03.003.

Nam, B.H., Park, K. and Kim, Y.J. (2024). "Prediction of karst sinkhole collapse using a decision-tree (DT) classifier", *Geomech. Eng.*, **36**(5), 441-453. https://doi.org/10.12989/gae.2024.36.5.441.

Nam, B.H. and Shamet, R. (2020), "A preliminary sinkhole raveling chart", *Eng. Geol.*, **268**, 105513. https://doi.org/10.1016/j.enggeo.2020.105513.

Nof, R.N., Abelson, M., Raz, E., Magen, Y., Atzori, S., Salvi, S. and Baer, G. (2019). "SAR interferometry for sinkhole early warning and susceptibility assessment along the Dead Sea, Israel", *Remote Sens*., 11(1), 89. https://doi.org/10.3390/rs11010089

Nur, A.S., Kim, Y.J., Lee, J. and Lee, C.W. (2023), "Spatial prediction of wildfire susceptibility using hybrid machine learning models based on support vector regression in Sydney, Australia", *Remote Sens.*, **15**(3), 760. https://doi.org/10.3390/rs15030760.

Nur, A.S., Nam, B.H., Choi, S. and Kim, Y.J. (2024), "Monitoring of ground subsidence using PS-InSAR technique in the Southeast Texas (SETX) Region", *Int. J. Geo-Eng*., **15**(1), 13. https://doi.org/10.1186/s40703-024-00215-3.

Osmanoğlu, B., Sunar, F., Wdowinski, S. and Cabral-Cano, E. (2016), "Time series analysis of InSAR data: Methods and trends", *ISPRS J. Photogramm*., **115**, 90-102. https://doi.org/10.1016/j.isprsjprs.2015.10.003.

Panahi, M., Sadhasivam, N., Pourghasemi, H.R., Rezaie, F. and Lee, S. (2020), "Spatial prediction of groundwater potential mapping based on convolutional neural network (CNN) and support vector regression (SVR)", *J. Hydrol.*, **588**, 125033. https://doi.org/10.1016/j.jhydrol.2020.125033.

Pedregosa, F., Varoquaux, G., Gramfort, A., Michel, V., Thirion, B., Grisel, O., Blondel, M., Prettenhofer, P., Weiss, R. and Dubourg, V. (2011), "Scikit-learn: Machine learning in Python", *J. Mach. Learn. Res*., **12**, 2825-2830.

Prete, S.D.D.C. (2010), "Collapse sinkholes in Campania (southern Italy): predisposing factors, genetic hypothesis and susceptibility", *Zeitschrift Für Geomorphologie*, Supplementary Issues, **54**(2), 259-284. https://doi.org/10.1127/0372-8854/2010/0054S2-0014.

Song, S.Y., Kim, B., Cho, A., Jeong, J., Lee, D. and Nam, M.J. (2023), "Electrical resistivity survey and interpretation considering excavation effects for the detection of loose ground in urban area", *Geomech. Eng*., **35**(2), 109-119. https://doi.org/10.12989/gae.2023.35.2.109.

Shamet, R., Nam, B.H. and Yoon, H. (2021), "An empirically developed CPT-based assessment method for characterization of sinkhole vulnerability in Florida Karst", IFCEE 2021, 297-307. https://doi.org/10.1061/9780784483428.031.

Tacim, G., Posluk, E. and Gokceoglu, C. (2023), "Importance of grouting for tunneling in karstic and complex environment (a case study from Türkiye)", *Int. J. Geo-Eng*., **14**(1), 6. https://doi.org/10.1186/s40703-023-00183-0.

Talib, O.C., Shimon, W., Sarah, K. and Tonian, R. (2022), "Detection of sinkhole activity in West-Central Florida using InSAR time series observations", *Remote Sens. Environ*., **269**, 112793. https://doi.org/10.1016/j.rse.2021.112793.

Theron, A. and Engelbrecht, J. (2018), "The role of earth observation, with a focus on SAR interferometry, for sinkhole hazard assessment". *Remote Sens.*, **10**(10), 1506. https://doi.org/10.3390/rs10101506.

Theron, A., Engelbrecht, J., Kemp, J., Kleynhans, W. and Turnbull, T. (2017), "Detection of sinkhole precursors through SAR interferometry: Radar and geological considerations", *IEEE Geosci. Remote Sens. Lett*., **14**(6), 871-875. https://doi.org/10.1109/LGRS.2017.2684905.

Wang, S.C. (2003), "Artificial neural network", Interdisciplinary Computing in Java Programming, 81-100.

Wang, Z., Da Cunha, C., Ritou, M. and Furet, B. (2019), "Comparison of K-means and GMM methods for contextual clustering in HSM", *Procedia Manufact*., **28**, 154-159. https://doi.org/10.1016/j.promfg.2018.12.025.

Weary, D. (2015), "The cost of Karst subsidence and sinkhole collapse in the united states compared with other natural hazards", Sinkholes and the Engineering and Environmental Impacts of Karst: *Proceedings of the 14th Multidisciplinary Conference*, 433–446. https://doi.org/10.5038/9780991000951.1062.

Zhang, Y., Jiao, Y.Y., He, L.L., Tan, F., Zhu, H.M., Wei, H.L. and Zhang, Q.B. (2024), "Susceptibility mapping and risk assessment of urban sinkholes based on grey system theory", *Tunn. Undergr. Sp. Tech*., **152**, 105893. https://doi.org/10.1016/j.tust.2024.105893.

Zhu, J., Nolte, A. M., Jacobs, N. and Ye, M. (2020), "Using machine learning to identify karst sinkholes from LiDAR-derived topographic depressions in the bluegrass region of Kentucky", *J. Hydrol*,, **588**, 125049. https://doi.org/10.1016/j.jhydrol.2020.125049.